Hydrogeology Journal (2023) 31:1405–1423
https://doi.org/10.1007/s10040-023-02681-y

REPORT

Assessment of changes in regional groundwater levels through spatio-temporal kriging: application to the southern Basin of Mexico aquifer system

H. E. Júnez-Ferreira[1] · M. A. Hernández-Hernández[2] · G. S. Herrera[3] · J. González-Trinidad[1] · C. Cappello[4] · S. Maggio[4] · S. De Iaco[4,5,6]

Received: 24 October 2022 / Accepted: 6 July 2023 / Published online: 1 September 2023

Abstract

A common approach for calculating the spatial distribution of groundwater level changes consists in choosing a set of different times, interpolating the groundwater level data available at each time over a spatial grid, and then calculating changes in each period by subtracting the interpolated values for these times. However, this can produce misleading results when the data are available in different positions for consecutive times. This paper presents an alternative procedure based on the interpolation of the groundwater level with spatio-temporal kriging, the assessment of the temporal groundwater elevation changes over a regional semiconfined aquifer, and the estimation of their error standard deviations. A comparative analysis of cross-validation results and error standard deviations provides a quantitative measure of the superiority of the introduced approach with respect to the one given in the literature. Moreover, the spatio-temporal case produces more reasonable estimates than the spatial kriging, notably fewer extreme recoveries and drawdowns, in an area under high water stress, such as the upper aquifer of the southern part of the Basin of Mexico aquifer system.

Keywords Geostatistics · Groundwater development · Groundwater flow · Spatio-temporal kriging · Mexico

Introduction

Analyzing groundwater level changes at the regional scale constitutes an essential tool for evaluating the response of aquifers to climatic variation and management policies. Its correct interpretation is critical for hydrogeologists since it provides information about groundwater storage changes for a specific period and can also trigger warning alarms regarding undesirable water level decline rates. Thus, it represents a valuable asset to better understanding groundwater dynamics. The reliability of the spatial distribution of groundwater level changes for a given period depends on the quantity

Published in the special issue "Geostatistics and hydrogeology".

✉ G. S. Herrera
ghz@igeofisica.unam.mx

H. E. Júnez-Ferreira
hejunez@uaz.edu.mx

M. A. Hernández-Hernández
malbher@igeofisica.unam.mx

J. González-Trinidad
jgonza@uaz.edu.mx

C. Cappello
claudia.cappello@unisalento.it

S. Maggio
sabrina.maggio@unisalento.it

S. De Iaco
sandra.deiaco@unisalento.it

[1] Licenciatura en Ciencia y Tecnología del Agua y Doctorado en Ciencias de la Ingeniería, Universidad Autónoma de Zacatecas "Francisco García Salinas", Zacatecas, Mexico

[2] Investigador por México CONAHCYT - Instituto de Geofísica, Universidad Nacional Autónoma de México, Mexico City, Mexico

[3] Instituto de Geofísica, Universidad Nacional Autónoma de México, Mexico City, Mexico

[4] Department of Economic Sciences, University of Salento, Lecce, Italy

[5] National Future Center of Biodiversity, Palermo, Italy

[6] National Centre for HPC, Big Data and Quantum Computing, Bologna, Italy

and quality of the available data at the initial and final times of the period. Measurement errors, differences between the number and position of monitored piezometers or wells at the initial and the final monitoring dates, and the estimation method used to calculate the variations are among the largest sources of estimate uncertainty.

Evaluation of the spatial distribution of temporal changes in groundwater levels can be done by using depth to groundwater (DG) or groundwater elevation (GE) estimates. Among the different existing approaches to estimate DG and GE, the geostatistical one has often been used with good results.

Table 1 summarizes the papers that have focused on estimating DG, GE, and temporal changes in groundwater levels using geostatistics, including this one. The papers are reported according to three categories, depending on their approach: spatial and temporal separately, multivariate, and spatio-temporal (ST). They are ordered chronologically within each category. For the first kind of analysis, groundwater levels at different times are considered independent spatial random fields, and groundwater levels at different positions are treated as independent temporal series. In the multivariate analysis groundwater levels at each time are figured as different random fields, temporally correlated. Finally, the ST analysis considers groundwater levels at all positions and times as a spatially and temporally correlated random field. Only the last two kinds of analysis account for the ST correlations of groundwater levels.

Most geostatistical analyses of groundwater changes over time were applied to unconfined porous aquifers and, just recently, to semiconfined aquifers, karstic aquifers, and aquifer systems or several aquifers laterally connected.

Concerning spatial scales, there are three ranges: local (10 km^2), medium (10^2 km^2), and regional (10^3 km^2). It is important to note that it has been only recently that ST analyses on regional scales have been published. The density of positions per kilometer for the spatial analyses or the average spatial density for the ST analyses is reported in Table 1 as a measure of the scarcity of spatial data.

Two kriging methods were applied for the ST approach, ordinary and residual ordinary kriging. Concerning the ST structure assumed for the covariances, three kinds have been used in the reported works, product-sum, sum-metric, and Spartan. Also, a non-Euclidean distance was used to represent better the effects of contrasting hydraulic conductivities on hydraulic levels of aquifers connected laterally.

The only works that used a ST approach and reported groundwater level temporal changes are Ruybal et al. (2019a, 2019b). The temporal changes for the reported periods were calculated by subtracting the groundwater elevation (GE) estimates, using ST kriging, for the initial and final dates of the period. However, they did not report standard deviation (SD) or variances for groundwater level change errors. On the other hand, of those using spatial kriging to estimate groundwater level changes, only Ahmadi and Sedghamiz (2007) included the spatial distribution of SD. For each well, DG in the final year was subtracted from that in the initial year, and afterward, interpolation was done using ordinary kriging.

Differently from the other contributions, this paper assesses the spatial distribution of the temporal changes in groundwater levels through spatial and ST kriging for the upper aquifer of the Southern part of the Basin of Mexico Aquifer System (SBMAS) and their estimate error standard deviations. It is worth noting that the standard deviations of the ST kriging estimate differences are presented for the first time. This work also contributes to establish a systematic procedure for ST geostatistical analysis by using the non-separability index for the choice of the appropriate class of the ST variogram model that fits the surface of the empirical variogram (De Iaco and Posa 2013; Cappello et al. 2018). Concerning the characteristics of the application, this is one of the few works that apply ST geostatistics to a semiconfined aquifer under high water stress on a regional scale.

The structure of this paper is as follows. "Materials and methods" section presents the background for the spatial and the ST geostatistical-based approaches used in this research to estimate the GE level and the spatial distribution of groundwater-level temporal changes. "Main characteristics of the study area" section describes the main demographic, climatic, physical, and hydrogeological features of the region where the analysis is done and the conceptual model of the groundwater flow dynamics. "Geostatistical modeling" section presents spatial and ST geostatistical analyses for the GE data and compares the GE's spatial and ST kriging estimates and their changes between two specified years. Finally, the last two sections provide some remarks on the obtained results compared with previous studies and some conclusions regarding open issues.

Materials and methods

The spatial distribution of the temporal changes in GE for a given period is calculated as the difference in the values of the GE spatial interpolations for the period's initial and final dates. One of the most common alternatives for interpolating GE for a given date is using spatial geostatistical methods such as ordinary kriging. However, when data at different sample locations for the initial and final dates are available and used as input for interpolations, inconsistencies in the spatial distribution of temporal changes can be presented

Table 1 Summary of reviewed papers on geostatistical methods for estimating groundwater elevation (GE), depth to groundwater (DG), and its temporal changes, and the present study

Reference	Location	Aquifer type	Extent (km^2)	Data frequency	Number of data	Kind of analysis	Method	ST structure	Period
Ahmadi and Sedghamiz (2007)	Darab plain, Iran	Unconfined	175	Monthly DG	39 positions (SD 0.223), 144 months	S&T	Spatial - Ordinary kriging, Temporal - Universal kriging	-	12 years
Ta'Any et al. (2009)	Amman-Zarqa basin, Jordan	Unconfined	4,049	Monthly DG	34 positions (SD 0.008), 144 months	S&T	Spatial - Ordinary kriging, Temporal - Correlogram analysis	-	12 years
Sun et al. (2009)	Minqin oasis, northwest China	Not specified	2,868	Monthly DG	48 positions (SD 0.017), 264 months	S&T	Inverse distance weighting, radial basis function; ordinary, simple, and universal kriging	-	22 years
Mendoza-Cázares and Herrera-Zamarrón (2007)	Valle de Querétaro, Central Mexico	Predominately unconfined	426	Yearly GE	3 years (89, 112, and 75 positions, ASD 0.216)	S&M	Residual ordinary cokriging	Linear coregionalization	3 years
Mendoza-Cázares and Herrera-Zamarrón (2010)	Valle de Querétaro, Central Mexico	Predominately unconfined	426	Yearly GE	1292 data, 65 average positions per year (ASD 0.152)	ST	Residual ordinary kriging	Product-sum	24 years
Varouchakis (2018)	Mires Basin, Crete, Greece	Unconfined	2	Monthly GE	11 positions (SD 5.5), 84 months	ST	Ordinary kriging	Product & product-sum	7 years
Varouchakis et al. (2019)	Mires Basin, Crete, Greece	Unconfined	3	Bi annual GE	10 positions (SD 3.3), 68 data each	ST	Ordinary and residual ordinary kriging. Variogram functions with non-Euclidean distance metric. Bayesian Bootstrap to quantify uncertainty	Product-sum & Spartan	34 years
Ruybal et al. (2019a)	Arapahoe aquifer, Greater Denver metro area, Colorado, USA	Unconfined and Semiconfined	11,135	Monthly and yearly GE	118 positions (SD 0.01)	S&ST	Ordinary and residual ordinary kriging	Sum-metric	27 years
Varouchakis et al. (2022)	Island of Crete, Greece	Unconfined porous and karstic	8,336	Bi annual GE	311 positions (SD 0.037), 18 data each	ST	Bayesian method combining machine learning and regression	Spartan	9 years
Present study	Upper aquifer of the SBMAS, Mexico	Unconfined and Semiconfined	2,104	Yearly GE	67 average positions per year (ASD 0.084), 3,699 data	S&ST	Ordinary and residual ordinary kriging	Product-sum	20 years

S&T Spatial and temporal separately, S Spatial, M multivariate, ST Spatio-temporal, SD Spatial Density, ASD Average Spatial Density

since kriging produces smoothed estimates depending on data availability.

In the present paper, the spatial distribution of temporal changes in GE for the upper aquifer of the SBMAS is calculated from 2002 to 2007 using spatial and ST geostatistical techniques. Subsequently, the GE differences are statistically compared.

For the spatial approach, the GE map of each year is estimated using data from the same year only. GE is assumed to be a finite realization of a real-valued spatial random field $\{Z(\mathbf{s})\colon \mathbf{s} \in D\}$ where $\mathbf{s}$ is a spatial location and $D \subseteq \mathbb{R}^d$ $(d \geq 2)$ is the spatial domain. The random field is assumed to be second-order stationary, with an expected value constant over the domain, i.e., $E[Z(\mathbf{s})] = m$, $\forall \mathbf{s} \in D$, and a covariance which is only dependent on the separation vector $\mathbf{h}$, i.e., $C(\mathbf{h}) = E[Z(\mathbf{s}+\mathbf{h}) - Z(\mathbf{s})] - m^2$, $\mathbf{s}, \mathbf{s}+\mathbf{h} \in D$. Under second order stationarity, this relationship between covariogram and variogram holds: $C(\mathbf{h}) = C(\mathbf{0}) - \gamma(\mathbf{h})$.

Estimation problems can be addressed by resorting to the kriging method, such as ordinary kriging, which is used when the expected value is assumed constant and unknown (Chilès and Delfiner 2012). Applying kriging for estimation purposes implies knowledge of a spatial correlation model. Thus, it is necessary to estimate and model a measure of spatial correlation, like the variogram, based on the sample data.

It is important to recall that the variogram model selected to fit the empirical variogram must be conditionally negative definite; for this reason, well-known functions, i.e., spherical, exponential, Gaussian, and hole effect, which satisfy this condition, are widely used (Journel and Huijbregts 1978; Cressie 1993; Christakos 1984).

For the ST approach, data from the whole dataset are used to obtain the estimates for the initial and final years of the period fixed for computing the variation. In a ST context, the observations of the GE are assumed to be a finite realization of a real-valued ST random field, which is denoted with $\{Z(\mathbf{s},t)\colon (\mathbf{s},t) \in D \times T\}$, where $(\mathbf{s},t)$ is a ST location, $D \subseteq \mathbb{R}^d$ $(d \geq 2)$ is the spatial domain, and $T \subseteq \mathbb{R}$ is the temporal domain. Under second-order stationarity, the random function Z is characterized by a constant expected value, i.e., $E[Z(\mathbf{s},t)] = m$, $\forall (\mathbf{s},t) \in D \times T$, and a covariance or a variogram function which depends on the ST lag $(\mathbf{h}_s, h_t)$, i.e., $C_{st}(\mathbf{s},t;\mathbf{s}',t') = C_{st}(\mathbf{h}_s, h_t)$, where $\mathbf{h}_s = (\mathbf{s}-\mathbf{s}')$ and $h_t = (t-t')$. Similarly to the spatial domain, the following relationship between covariogram and variogram holds: $C_{st}(\mathbf{h}_s, h_t) = C_{st}(\mathbf{0},0) - \gamma_{st}(\mathbf{h}_s, h_t)$. In order to face estimation problems in space-time, the ordinary kriging estimator $\widehat{Z}(\mathbf{s},t)$ can be used (Chilès and Delfiner 2012).

As in the spatial case, the ST kriging system requires knowledge of the variogram model. For this aim, structural analysis for variogram estimation and modeling has to be conducted. To model the sample ST variogram, the literature offers a wide list of classes of variogram functions to choose from. In particular, the product class, where space and time are treated separately (Rodriguez-Iturbe and Mejía 1974; Posa 1993) has represented the base to generate other parametric families of ST variogram or covariance functions (De Iaco et al. 2001; Ma 2002, 2003). Otherwise, various classes of non-separable ST models were also developed by Cressie and Huang (1999), Gneiting (2002), De Iaco et al. (2002), among others.

In this context, the non-separability index, firstly introduced by Rodriguez and Diggle (2010) and then generalized by De Iaco and Posa (2013), was proposed in the literature in order to choose the appropriate class of model for describing the empirical ST correlation structure. After the selection of the appropriate class of ST variogram or covariance model and the estimation of the corresponding parameters, the specific model can be used for prediction purposes.

In the following the main notions concerning the non-separability index and the product-sum model will be recalled. The focus on the product-sum model is justified since its type of non-separability is consistent with the one shown by the empirical ST correlation structure of the GE data under study.

The non-separability index and its interpretation

In the literature, various possible types of non-separability for ST covariance functions have been provided. In De Iaco and Posa (2013) the definition of non-separability was adequately detailed and furtherly tested in Cappello et al. (2018). By recalling the definition in De Iaco and Posa (2013), the non-separability index for a ST stationary covariance function $C_{st}(\mathbf{h}_s, h_t; \boldsymbol{\Theta})$ depending on a vector of parameters $\boldsymbol{\Theta}$, is expressed as follows:

$$r(\mathbf{h}_s, h_t; \boldsymbol{\Theta}) = \frac{\rho_{st}(\mathbf{h}_s, h_t; \boldsymbol{\Theta})}{\rho_{st}(\mathbf{h}_s, 0; \boldsymbol{\Theta})\rho_{st}(\mathbf{0}, h_t; \boldsymbol{\Theta})} \tag{1}$$

where $\rho_{st}(\mathbf{h}_s, h_t; \boldsymbol{\Theta})$ is the spatial-temporal correlation function, satisfying the conditions $\rho_{st}(\mathbf{h}_s, h_t; \boldsymbol{\Theta}) > 0$, $\rho_{st}(\mathbf{h}_s, 0; \boldsymbol{\Theta}) > 0$ and $\rho_{st}(\mathbf{0}, h_t; \boldsymbol{\Theta}) > 0$.

According to this definition, a ST stationary covariance function C_{st} is:

- uniformly positive non-separable, if $r(\mathbf{h}_s, h_t; \boldsymbol{\Theta}) > 1$ for all $(\mathbf{h}_s, h_t) \in D \times T \subseteq \mathbb{R}^{d+1}$, $(\mathbf{h}_s, h_t) \neq (\mathbf{0}, 0)$ and for all $\boldsymbol{\Theta}$,
- pointwise positive non-separable at $(\mathbf{h}_s, h_t; \boldsymbol{\Theta})$, if $r(\mathbf{h}_s, h_t; \boldsymbol{\Theta}) > 1$.

By changing the direction of the above inequalities, uniform negative non-separability or poitwise negative non-separability are defined.

In variogram form, the empirical non-separability index is computed as reported below:

$$\hat{r}(\mathbf{h}_s, h_t; \Theta) = \frac{\hat{C}_{st}(\mathbf{0},0) - \hat{\gamma}_{st}(\mathbf{h}_s, h_t)}{[\hat{C}_{st}(\mathbf{0},0) - \hat{\gamma}_{st}(\mathbf{h}_s,0)][\hat{C}_{st}(\mathbf{0},0) - \hat{\gamma}_{st}(\mathbf{0}, h_t)]} \cdot \frac{1}{\hat{C}_{st}(\mathbf{0},0)} \tag{2}$$

where $\hat{C}_{st}(\mathbf{0},0)$ is the estimated variance, $\hat{\gamma}_{st}(\mathbf{h}_s, h_t)$ is the empirical ST variogram, $\hat{\gamma}_{st}(\mathbf{h}_s,0)$ and $\hat{\gamma}_{st}(\mathbf{0}, h_t)$ are the purely sample spatial and temporal variograms, respectively.

De Iaco and Posa (2013) proposed a classification of some well known classes of covariance models, on the basis of the above mentioned definition. Among them, the product-sum covariance model, selected in the case study described hereafter, belongs to the class of models with uniformly negative non-separability.

From a computational point of view, box plots of empirical non-separability ratio, computed for both spatial and temporal lags, can help to efficiently identify the types of non-separability. The R package `covatest` (Cappello et al. 2020) is used to assess the non-separability, characterizing the ST correlation structure of the data under study.

The product-sum ST model

The product-sum model (De Cesare et al. 2001; De Iaco et al. 2001) can be formalized in terms of the covariance function as follows:

$$C_{st}(\mathbf{h}_s, h_t) = k_1 C_s(\mathbf{h}_s) C_t(h_t) + k_2 C_s(\mathbf{h}_s) + k_3 C_t(h_t) \tag{3}$$

with $k_1 > 0, k_2 \geq 0, k_3 \geq 0$ and where C_t and C_s are valid temporal and spatial covariance models, respectively.

As widely detailed in De Iaco et al. (2001), the Eq. (3) can be written in variogram form:

$$\begin{aligned}\gamma_{st}(\mathbf{h}_s, h_t) = {} & [k_2 + k_1 C_t(0)]\gamma_s(\mathbf{h}_s) + [k_3 + k_1 C_s(\mathbf{0})]\gamma_t(h_t) \\ & - k_1 \gamma_s(\mathbf{h}_s)\gamma_t(h_t)\end{aligned} \tag{4}$$

where γ_s and γ_t represent valid spatial and temporal variogram models, $C_s(\mathbf{0})$ and $C_t(0)$ correspond to the sill values.

By applying the variogram property according to which the value of the variogram at the origin is zero, it implies that:

$$\gamma_{st}(\mathbf{h}_s, 0) = [k_2 + k_1 C_t(0)]\gamma_s(\mathbf{h}_s) = k_s \gamma_s(\mathbf{h}_s) \tag{5}$$

and

$$\gamma_{st}(\mathbf{0}, h_t) = [k_3 + k_1 C_s(\mathbf{0})]\gamma_t(h_t) = k_t \gamma_t(h_t) \tag{6}$$

where k_s and k_t satisfy the following equations:

$$k_2 + k_1 C_t(0) = k_s \tag{7}$$

$$k_3 + k_1 C_s(\mathbf{0}) = k_t \tag{8}$$

The coefficients k_1, k_2, and k_3 can be obtained as reported below:

$$k_1 = \frac{k_s C_s(\mathbf{0}) + k_t C_t(0) - C_{st}(\mathbf{0},0)}{C_s(\mathbf{0}) C_t(0)} \tag{9}$$

$$k_2 = \frac{C_{st}(\mathbf{0},0) - k_t C_t(0)}{C_s(\mathbf{0})} \tag{10}$$

$$k_3 = \frac{C_{st}(\mathbf{0},0) - k_s C_s(\mathbf{0})}{C_t(0)} \tag{11}$$

where $C_{st}(\mathbf{0},0)$ is called global sill.

By recalling the Eqs. (5) and (6), the Eq. (4) can be expressed as follows:

$$\gamma_{st}(\mathbf{h}_s, h_t) = \gamma_{st}(\mathbf{h}_s, 0) + \gamma_{st}(\mathbf{0}, h_t) - k\gamma_{st}(\mathbf{h}_s, 0)\gamma_{st}(\mathbf{0}, h_t) \tag{12}$$

where $k = \dfrac{k_1}{k_s k_t} = \dfrac{k_s C_s(\mathbf{0}) + k_t C_t(0) - C_{st}(\mathbf{0},0)}{k_s C_s(\mathbf{0}) k_t C_t(0)}$

As proved in De Iaco et al. (2001), this simplified form of $\gamma_{st}(\mathbf{h}_s, h_t)$ includes only k as the parameter, which depends on the global sill value $C_{st}(\mathbf{0},0)$. The Eq. (12) is admissible if and only if the following condition for k is satisfied:

$$0 < k \leq \frac{1}{\max\{\text{sill } \gamma_{st}(\mathbf{h}_s, 0),\ \text{sill } \gamma_{st}(\mathbf{0}, h_t)\}} \tag{13}$$

Further details are available in De Iaco et al. (2001).

Drift

When the expected value of a ST random function Z depends on the space location, on time or both, the second-order stationarity hypothesis is not satisfied for Z. In that case, the random function can be expressed as:

$$Z(\mathbf{s}, t) = m(\mathbf{s}, t) + R(\mathbf{s}, t) \tag{14}$$

where $m(\mathbf{s}, t)$ represents a deterministic function (known as drift) and $R(\mathbf{s}, t)$, known as the residual, is supposed to be a zero mean second-order stationary ST random function modeling the space-time fluctuations around $m(\mathbf{s}, t)$ (Kyriakidis and Journel 1999). To represent the function $m(\mathbf{s}, t)$, a trend surface (typically polynomial functions) can be obtained by a least-squares fit to the data. In this way, zero mean stationary data (residuals) are obtained and used to calculate the variogram.

Main characteristics of the study area

Mexico City is settled in the southern part of the Basin of Mexico (BM) (Fig. 1), which is surrounded by volcanic sierras with altitudes higher than 3,500 meters above sea level (masl, from now on, m) and with alluvial fans, flood plains composed by sand, silt, clay and volcanic materials deposited in the central part of the valley (Arce et al. 2019). The BM is bounded to the south by the Sierra Ajusco-Chichinautzin, at the east by the Sierra Nevada, at the west by the Sierra de las Cruces and north by the Pachuca Sierra. It is considered an endorheic basin with no natural outflows; the natural drainage initially converged to the inferior part of the basin, giving origin to a system of 5 lakes with superficial and groundwater inputs (Herrera and Dumars 1995). Most of the groundwater recharge happens in the surrounding ranges, producing surface and subsurface flows towards the center of the basin, which originally were discharged through springs in the mountain areas and through the bottom of the lakes, mixing with water coming from surrounding rivers (Carrillo-Rivera et al. 2008; Bücker et al. 2017).

During the Spanish colonial period (1521-1821), the basin underwent artificial modifications as part of human-induced changes in the hydrogeological system. These alterations included the construction of catchment and drying channels. Additionally, to control flooding and facilitate the urban expansion of the city, the five lakes originally present in the area until the mid-19th century were subsequently dried. In more recent times, a deep sewage system was developed, redirecting rainwater and wastewater from the basin to a neighboring basin located to the north in the state of Hidalgo (Herrera and Dumars 1995).

The metropolitan area of Mexico City extends over a large portion of the study area (3,985 km^2), and according to the 2020 population and housing census (INEGI 2022), more than 21 million inhabitants live there, comprising 17.3% of the country's total population. This anthropological change has influenced the local hydrology through the intensive demand for groundwater for urban and industrial supply, and through urbanization of the basin and modification of local weather patterns.

According to Ávila-Carrasco et al. (2023), on average, the cumulative annual rainfall is of the order of 700 mm, which is distributed irregularly. The highest precipitation (up to 1400 mm/year) occurs in the mountains and ranges, where forest and natural areas are still conserved, while the lowest precipitation (400 mm/year) occurs in the lower and the plain regions at the center of the study area, where most of the urbanization and impermeable areas are located. However, there is still a recharge

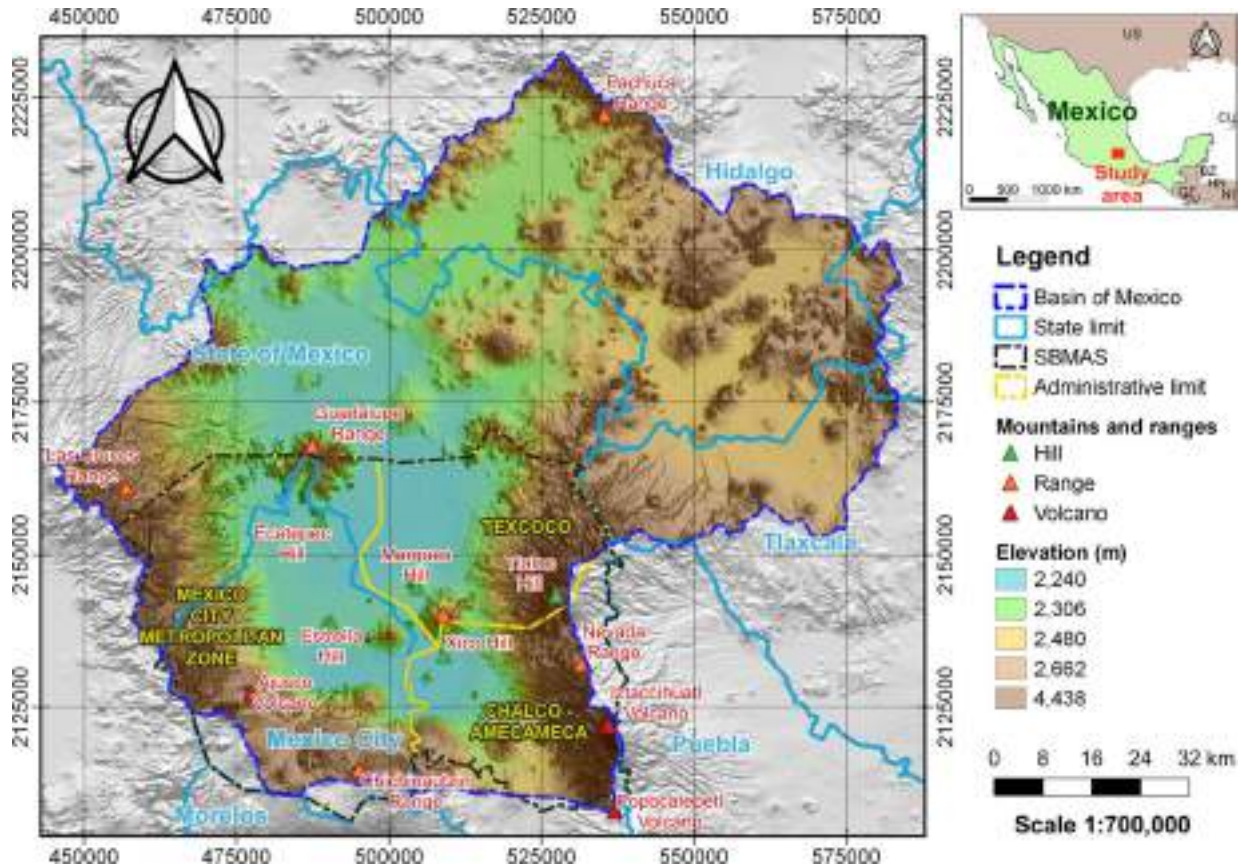

Fig. 1 Study area. Limit of the Basin of Mexico (BM) and the Southern Basin of Mexico Aquifer System (SBMAS)

input in the plain area, related to urban parks, channels, agricultural areas, flooding areas, and leakage from the water supply, and sewer systems. Regarding the changes in temperature, the highest values occur from April to May, and the lowest from November to February, with an average value of 21 °C, conditioning related parameters such as evapotranspiration, the available soil moisture, and the infiltration process.

Arce et al. (2019) cited several studies that have established the geology and stratigraphy of the BM during the past half century (Vázquez-Sánchez and Jaimes-Palomera, 1989), as well as recent studies defining the evolution of stratigraphic relations of the volcanic ranges around the basin. An initial hydrostratigraphic division was proposed by Mooser and Molina (1993) and subsequently modified by Ortega Guerrero et al. (1997), based on hydraulic properties of strata, conceptualizing the basin from the upper part to the bottom as: (1) low-permeability upper unit (LPUU, the upper aquitard), formed by Quaternary lacustrine clays, initially acting as a semi-confining unit for the permeable upper unit, with variable depth (5 to 130 m) and spatially placed where natural lakes were present, vertically connected to the lower unit and nowadays hydraulically disconnected in some areas due to decrease in piezometric level in the lower formation (Rudolph et al. 1991), having two recharge inputs (artificial recharge coming from sewer and supply systems, urban parks, channel, flooding areas, and natural recharge coming mainly from rain); (2) permeable upper unit (PUU, the upper aquifer in exploitation), formed by Quaternary-age alluvial and volcanic materials, as well as andesitic and dacitic Pliocene-age material with secondary porosity associated with fractures, and with 600 m depth on average having recharge inputs from leakage in the LPPU, natural recharge coming from rain inputs where the LPPU is not spatially present in the area and natural recharge from the surrounding mountains and ranges; (3) low-permeability lower unit (LPLU, the lower aquitard), formed by Oligocene and Eocene age igneous rocks and sandstones, shales and limestones of the Late Cretaceous age, with very low permeability and porosity (Mooser et al. 1996), considered as a hydraulic lower limit for the PUU; (4) permeable lower unit (PLU, the lower aquifer), formed by Early Cretaceous age rocks (limestones), with high permeability caused by intense fracturing and the presence of dissolution channels, considered as a potential aquifer with limited quality for urban consumption. A more detailed description of the hydrostratigraphic units is presented in Herrera-Zamarrón et al. (2020).

This study's efforts are centered on analyzing the temporal changes in GE in the PUU of the southern part of the BM aquifer system. Its limits are shown in Fig. 1. The National Commission of Water (Comisión Nacional del Agua, CONAGUA), which is the national entity in charge of water management, has divided the surface that comprises the LPUU and PUU hydrostratigraphic units (for administrative and legal purposes) into the Metropolitan Mexico City (MMC) Aquifer (2,104 km^2), the Texcoco Aquifer (934 km^2) and the Chalco-Amecameca Aquifer (947 km^2), corresponding to 41.5 percent of the total area of the BM (CONAGUA 2018).

Geostatistical modeling

This section will present a detailed description concerning the structural analyses of the GE data, the GE kriging estimates, and the GE changes between two specified years, for the spatial and ST cases.

Data description and exploratory analysis

The available GE data include annual observations for 21 years (from 1997 to 2017), distributed in the three administrative aquifers. They have been used to study, for the sake of simplicity, the temporal GE changes between the years 2002 and 2007; so that in the following, the complete dataset has been used for the ST analysis, while the spatial analysis has been conducted using GE data from the specified years.

Figure 2 shows the well positions in the dataset with special symbols in order to distinguish wells with data for 2002 and wells with data for 2007. The positions shown with black dots indicate wells with at least one data for the complete set of years. All the monitoring wells are production wells, which are irregularly distributed wells extracting water from the upper aquifer (PUU). Note that, although the measurements taken in active pumping wells could be heavily influenced by the exploitation strategy, a period of 24 hours (after the pump is turned off) must be considered for the GE measurements in the field according to the Mexican water agencies, so that the static groundwater level is reached. So, it is assumed that the GE measurements are static hydraulic heads.

In order to evaluate groundwater level differences in the valley area (where most of the wells are located), the raster layers are clipped by the topographic elevation of 2,300 m, shown with a blue dash line in Fig. 2, where the majority of the dataset is present.

It is worth pointing out that the average density of wells is larger compared with the regional studies reported in Table 1. However, while some areas and years lack information (for example, a broad area between the MMC and Texcoco aquifers), others are very dense. In some regions, 2002 and 2007 data can be complemented by data in other positions and years. For example, in the Chalco aquifer, several wells with data for 2007 lack data for 2002. Also, a portion of the MMC aquifer has no data for 2002 and 2007, but a significant amount of data for other years. So, depending on data availability, different spatial positions and GE values are used as data input for the spatial and ST analysis. The data from isolated wells outside the cropped area were removed.

The spatial and ST trends are modeled by using the second-degree polynomials (least-squares fitting), as shown

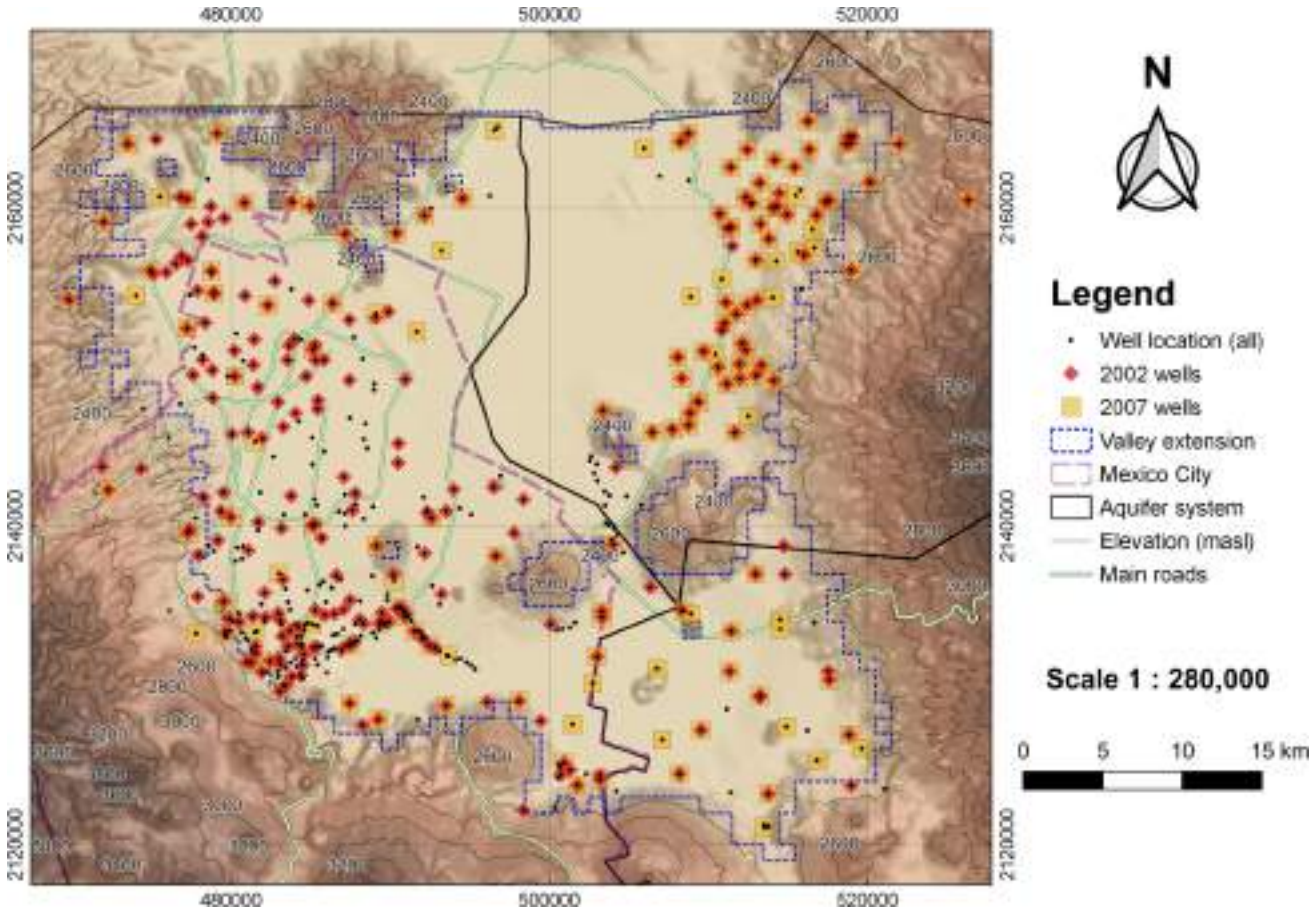

Fig. 2 Well locations for the complete set of data, from 1997 to 2017 (black dots). The position of wells with data for 2002 and 2007 are shown with different symbols (orange diamonds and yellow squares respectively). Where symbols overlap, data from more than one year concur

in Table 2. Note that the independent variables x and y are the UTM coordinates in the west-east and north-south axes, respectively, and t denotes the time in years. By analysing the basic statistics in Tables 3 and 4 a more symmetric distribution can be detected for the GE residuals. After removing the trend from the data, the residuals for both, the spatial and the ST case, are used in further steps.

The ST database comprises 3,699 measurements over time at 474 spatial locations, with an average of 176 locations per year. Concerning the data per well, eight have the longest time series (21 annual data corresponding to the analysis period), and the average data per well is 8.

Figure 3 shows the box plots of the GE residuals for each year, which are very similar in the period 1997-2010, then the dispersion of the data tends to increase from 2011 to 2017.

Structural analyses

In this step, the spatial and spatio-temporal variograms have been estimated and modeled. First of all, the omnidirectional spatial variograms of the residuals of GE for 2002 and 2007 have been estimated and the exponential models have been fitted to each of them, as shown in Fig. 4. The parameters of the selected spatial models are given in Table 5. It is worth

Table 2 Second degree polynomials adjusted to GE data

Dataset	Adjusted polynomial
247 GE (2002)	$m(x,y) = 325{,}674.488 - 0.059\,x + 5.938 \cdot 10^{-8}x^2 - 0.288\,y + 6.701 \cdot 10^{-8}y^2$
148 GE (2007)	$m(x,y) = 346{,}099.883 - 0.076\,x + 7.673 \cdot 10^{-8}x^2 - 0.303\,y + 7.047 \cdot 10^{-8}y^2$
3699 GE (1997-2017)	$m(x,y,t) = 343{,}073.483 - 0.072x + 7.206 \cdot 10^{-8}x^2 - 0.301\,y + 7.012 \cdot 10^{-8}y^2$ $-0.601\,t + 2.36 \cdot 10^{-3}t^2$

Table 3 Basic statistics of the GE data for years 2002 and 2007 (spatial case)

Variable	GE 2002	Residuals of GE 2002	GE 2007	Residuals of GE 2007
Number of data	247	247	148	148
Min (m)	2,141	-65.6	2,138.9	-48.4
Max (m)	2,286.9	71.3	2,285.5	75.5
Mean (m)	2,199	-0.003	2,200.5	-0.02
Std. Dev. (m)	21.9	18.2	24.1	19.2
Skewness	1.4	0.8	1.2	0.8
Kurtosis	5.2	4.7	4.4	4.3
1st Quartile (m)	2,185	-12.2	2,185.8	-11.12
Median (m)	2,192.9	-3.4	2,192.9	-3.2
3rd Quartile (m)	2,208.5	8.6	2,208.8	8.8

Table 4 Basic statistics of the GE data for the 1997-2007 period (spatio-temporal case)

Variable	GE 1997-2017	Residuals of GE 1997-2017
Number of data	3,699	3,699
Min (m)	2,129.28	-72.04
Max (m)	2,299.55	79.13
Mean (m)	2,198.34	-0.002
Std. Dev. (m)	22.98	18.45
Skewness	1.22	0.84
Kurtosis	1.85	1.48
1st Quartile (m)	2,182.82	-12.34
Median (m)	2,192.79	-3.88
3rd Quartile (m)	2,208.02	9.55

pointing out that no significant anisotropy has been detected from the sample spatial directional variograms.

By focusing on the ST case, the sample ST variogram of the residuals is obtained using 7 spatial and 14 temporal lags. The empirical surface of the ST variogram and the corresponding marginals, together with the marginal models, are illustrated in Fig. 5. In particular, the sample spatial and temporal variograms reported in Fig. 5b and c are drawn by using all the couples of data from the ST dataset.

The spatial lag size is 3 km, and each temporal lag has an extension of one year. Note that the spatial and temporal lags are fixed by considering the maximum distance among the sample locations and the length of the time series for each sample spatial point. The temporal marginal (variogram constructed using the time series) as well as the spatial marginal (variogram obtained using observations distributed in the spatial domain) are estimated and modeled before producing the ST variogram model.

In order to choose the appropriate class of ST variogram model, the sample non-separability ratios (2) are determined and classified by spatial and temporal lags (Fig. 6). From the box plots shown in Fig. 6 it is evident that the sample ratios are always less than one, which implies that a uniform negative non-separability is detected. Thus, the product-sum model is considered a suitable choice, since its theoretical type of non-separability is consistent with this evidence (De Iaco and Posa

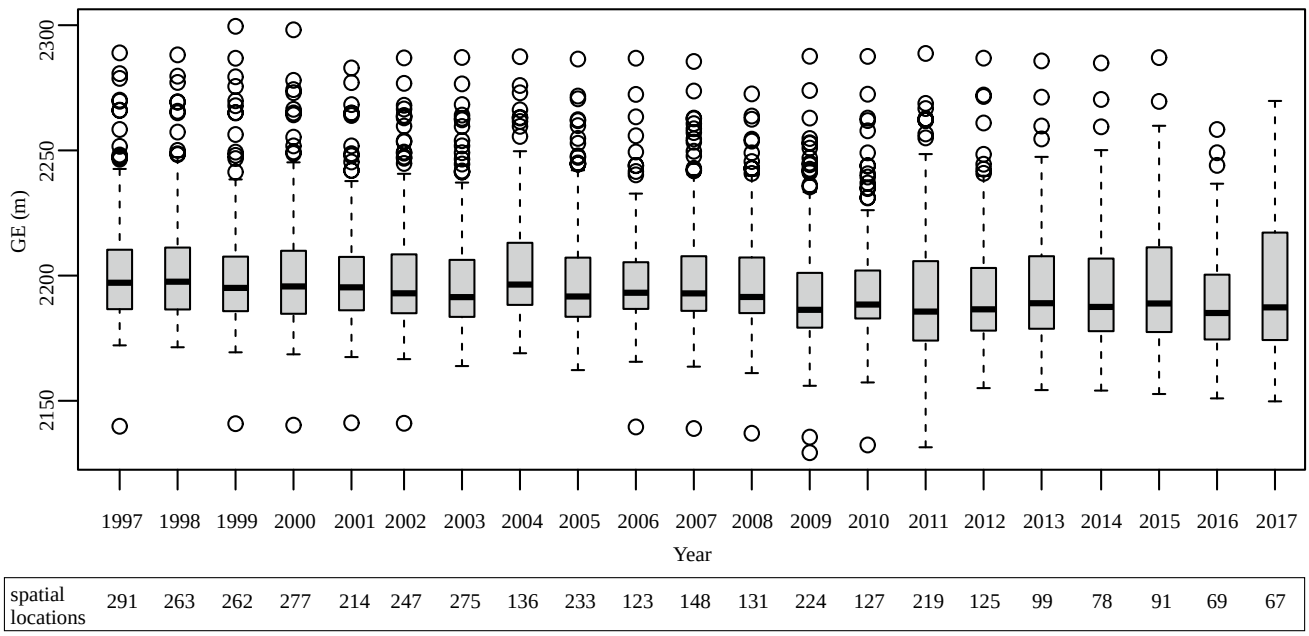

Fig. 3 Box plots of the GE for the years 1997-2017, together with the number of spatial locations per year

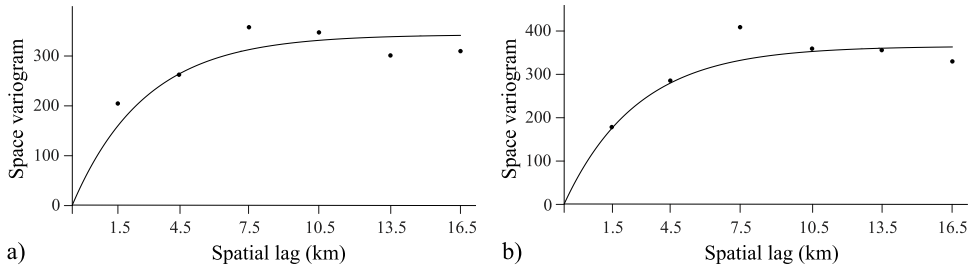

Fig. 4 Sample spatial variograms (black points) and its fitted variogram models (continuous line) of the GE residuals for the year **a** 2002, **b** 2007

Table 5 Parameter estimates of the selected spatial variogram models for the GE residuals

Year	Model	Nugget	Partial sill	Range
2002	Exponential	1 m^2	342 m^2	3100 m
2007	Exponential	1 m^2	364 m^2	3100 m

2013). Indeed, the type of non-separability of the product-sum is always uniformly negative, so that its non-separability index reflects the behavior of the empirical one.

The parameters of the selected ST product-sum model are shown in Table 6 and are such that the model is strictly positive definite (De Iaco and Posa 2018).

Cross-validation

In the following, the leave-one-out cross-validation procedure has been carried out in order to check the adequacy of the fitted spatial and ST models.

In Fig. 7 the scatter diagrams of the GE residuals and the estimated ones are shown, as well as the mean error (ME), the mean absolute error (MAE), the root mean square error (RMSE), the normalized root mean square error (NRMSE) and the Spearman correlation coefficients. For the spatial cases (Fig. 7a and c), the highest estimation error (overestimation) has been registered on the southwestern border of the domain and has been due to the presence of high observed residuals in its spatial neighborhood. In general, the dispersion of the cloud around the bisector has been caused by the reduced number of close neighbors for most of the estimates.

On the other hand, when using the ST approach for cross-validating the residuals for 2002 and 2007 (Fig. 7b and d)), the goodness of the estimates significantly increases. These statistics provide a quantitative measure of the obtained improvement, thanks to the high performance for the selected ST variogram model and the geometry of the sample points in ST.

Groundwater elevation estimates

In this section, spatial and ST kriging estimates are obtained on a grid with 1,000 m × 1,000 m cells size, covering a surface of 1,585 km^2 over the plain area (2,300 m), by adding the corresponding spatial or ST trend (Table 2) to the kriging residual estimates.

Figures 8 and 9 illustrate the spatial and ST kriging contour maps of the GEs and the distribution of the estimated values through their box plots and histograms for 2002 and 2007, respectively.

In the following, the corrections provided by using the ST approach with respect to the spatial one have been underlined.

In 2002 the GE minimum values are very similar (2,167 m and 2,172 m for the spatial and ST cases, respectively).

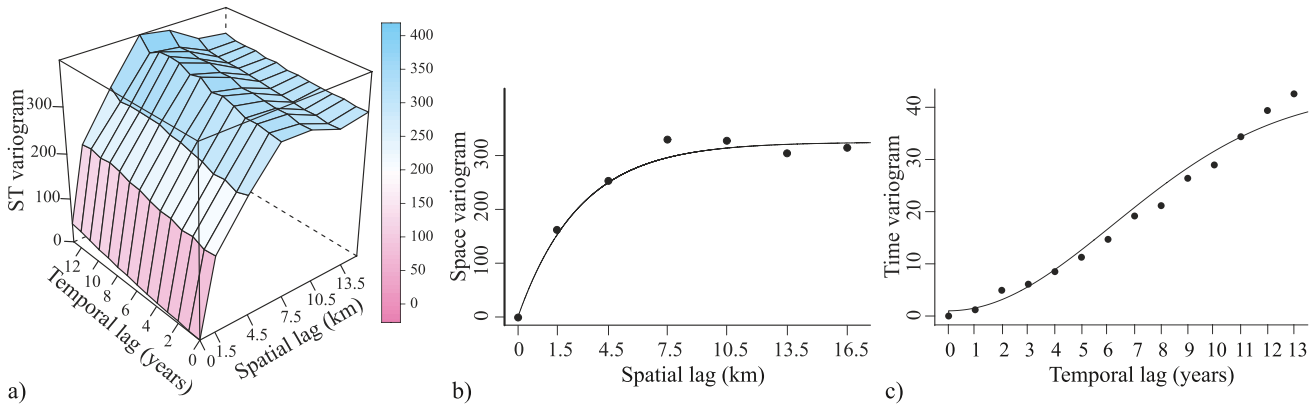

Fig. 5 **a** Sample spatio-temporal variogram surface, **b** sample spatial variogram (black points) and its fitted model (continuous line); **c** sample temporal variogram (black points) and its fitted model (continuous line), for the GE residuals within the period 1997-2017

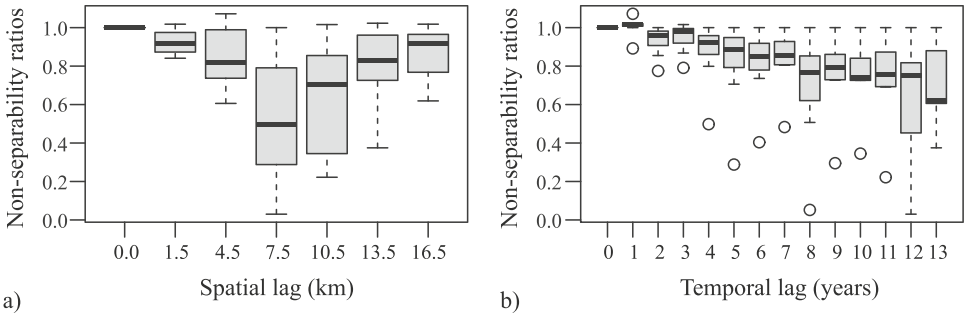

Fig. 6 Box plots of sample non-separability ratios grouped for **a** spatial and **b** temporal lags

Table 6 Parameter estimates of the selected spatio-temporal variogram model for the GE residuals within the 1997-2017 period

Model	Component	Nugget	Sill	Range
Exponential	Spatial	1 m^2	325 m^2	3100 m
Gaussian	Temporal	1 m^2	48 m^2	8 years
Product-sum	Global	1 m^2	368 m^2	-

However, there is a difference of 46 m between the maximum values (2,246 m and 2,292 m). Moreover, from the Fig. 8c and d, a moderately left-skewed distribution emerges for both the spatial and ST case, with a slightly wider left tail in the last one.

A similar behavior of the GE distributions can be found in 2007 (Fig. 9), with a difference of 11 m between the maximum values (2,259 m and 2,270 m) and a GE minimum value slightly smaller for the ST case than in the spatial one (2,163 m and 2,155 m).

Figure 8a and b for 2002 and Fig. 9a and b for 2007 show also that the highest GEs are close to the mountains in the periphery, as especially highlighted for the ST case. For 2002, the minimum values are found in the MMC aquifer, for both, the spatial and ST case. However, in the ST contour map, values lower than 2,180 m and more extended areas with values lower than 2,190 m are also found in the Texcoco aquifer.

For 2007, the minimum estimates are obtained in the Texcoco aquifer in both cases, although values lower than 2,180 m are more evident for the ST kriging, as shown in Fig. 9b.

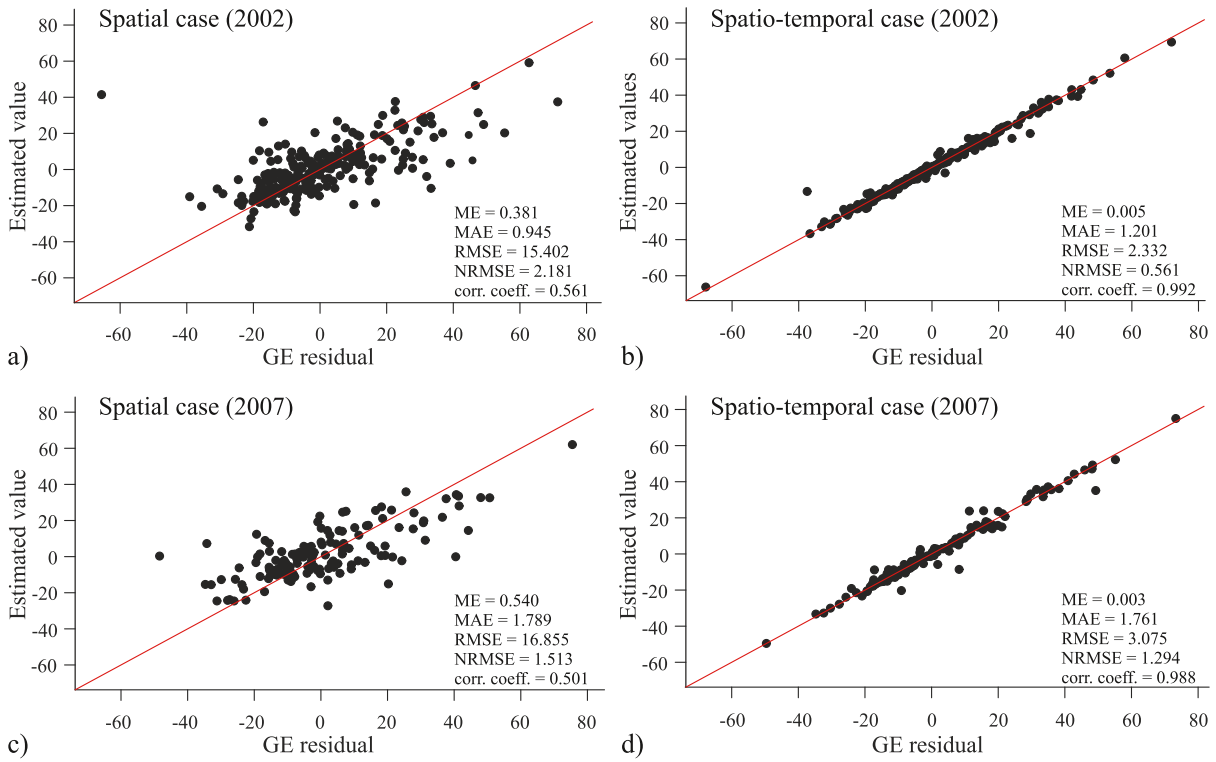

Fig. 7 Scatter plots of the cross-validation results of the GE residuals: true values versus estimated ones for the spatial and the spatio-temporal cases in the years 2002 (**a**), (**b**) and 2007 (**c**), (**d**)

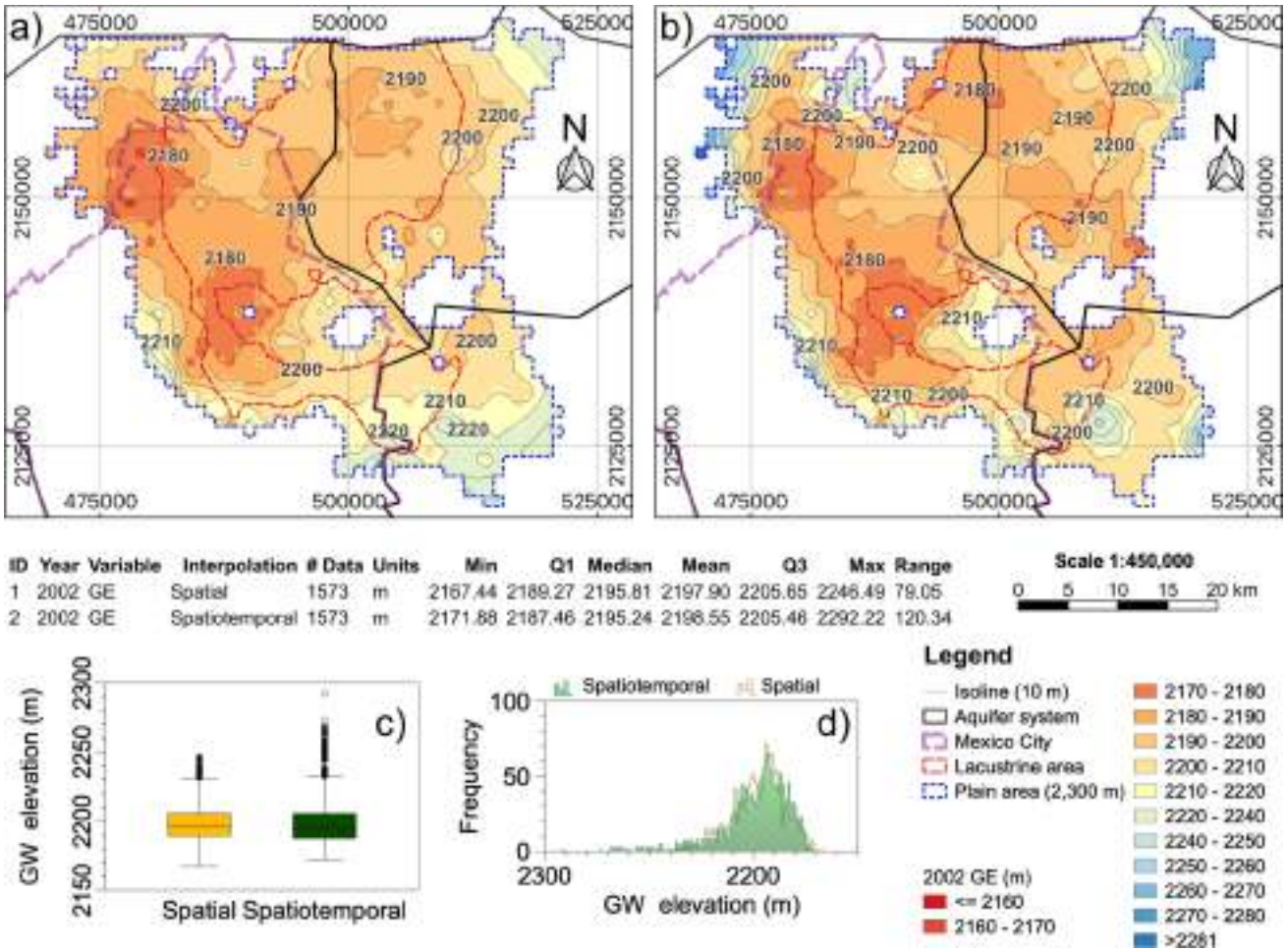

Fig. 8 Comparison of GE for the year 2002: **a** spatial and **b** ST kriging contour maps, **c** box plots and **d** histograms

Finally, a groundwater divide between the MMC and the Texcoco aquifers (close to the boundary of Mexico City), already recognized in previous works (Durazo and Farvolden 1989), is more clearly defined in the ST interpolations. Also, the Chalco aquifer has a consistent zone with high values in all the contour maps, which is better defined in the ST maps.

In addition, Fig. 10 illustrates the contour maps for the spatial and ST estimation error SD of GEs concerning the year 2002 and the distribution of their values through the box plots and histograms. It is worth pointing out that, for both the spatial and ST maps, the largest values are detected in the boundary between the MMC and the Texcoco aquifers, an area with almost no wells (see Fig. 2). Naturally, the smallest values are in the zones with a higher density of available data. The SD values tend to be smaller for the ST case with respect to the spatial one, due to the new geometry of the ST samples points and the ST model used to describe both the correlation in space and time together with the ST interaction. Indeed, 75% of the values are larger than 16.6 m in the spatial case, on the other hand, 75% of them are smaller than 14.5 m in the ST case. Moreover, by analysing Fig. 10c and d, it is evident that the estimation error SD distribution in the ST case is more symmetric than the one in the spatial case.

Similarly, Fig. 11 compares the contour maps of the spatial and ST estimation error SD of GEs for the year 2007. The general behavior of the distribution of the estimation error SD is similar to that of 2002, although those of the spatial case change more than the ST one. Note that the number of wells with data for 2007 are significantly less than for 2002, thus as expected, the ST estimates are more robust to the lack of data for one specific year.

Remark When comparing the spatial and ST interpolations, the main remarks are that the latter show larger areas characterized by the same low groundwater level (2,180 m) in both years. A groundwater divide between the MMC and the Texcoco aquifers is more clearly defined in the ST contour maps, which may be related to the large thickness of

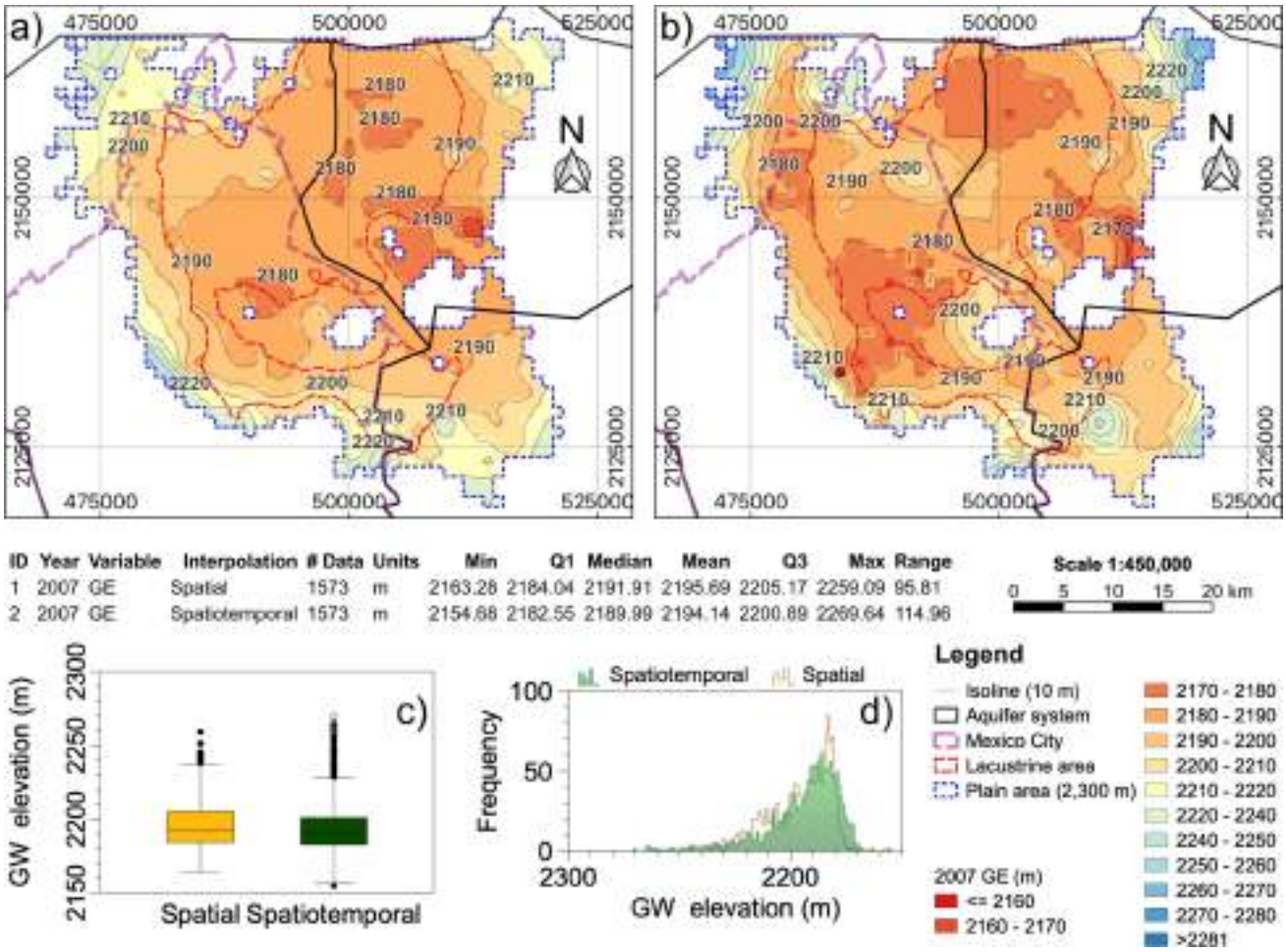

Fig. 9 Comparison of GE for the year 2007: **a** spatial and **b** ST kriging contour maps, **c** box plots, and **d** histograms

the aquitard in that area. Also, a zone consistently presents high values in the Chalco aquifer and is better defined in the ST maps. Considering the cumulative effect of historical withdrawals on the aquifer system, the cross-validation results, the lower SD error estimates for extended portions of the aquifer, and the more consistent error estimate SD distribution, it can be reasonably assumed that the ST estimates reflect more consistently the behavior of the natural response of a heavily pumped aquifer.

Groundwater level changes

In this section, the temporal changes of the GE, and their corresponding estimation error SD are estimated and mapped over the valley area (2,300 m) covered by the aquifer using a geographical information system. Finally, the results of the spatial and ST kriging approaches are compared and evaluated.

The spatial and ST kriging GE difference (GE in 2002 minus GE in 2007) over the aquifer and the distribution of their values through their box plots and histograms are shown in Fig. 12. While in the spatial case, the level differences are between -41.2 m and 33.7 m with a mean of 2.21 m and a median of 6.5 m, in the ST case, they are between -21.5 m and 55.1 m with a 4.3 m mean, very close to the median. As shown by the box plot (Fig. 12c), most of the estimated differences for the ST kriging highlight a GE recovery up to 5 m (-5 m in the reported results) and a drawdown up to 10 m, which seems to be reasonable for the studied area considering the GE evolution shown by the observed data at each well for the interval under study. From a direct cell count, 85.4% of the GE difference values present recovery up to 5 m (-5 m in terms of differences) or drawdown up to 10 m, for the ST kriging and only 45.8% for the spatial kriging.

In particular, in the ST case there are more extended areas with drawdowns of about 5 m, meaning that for the

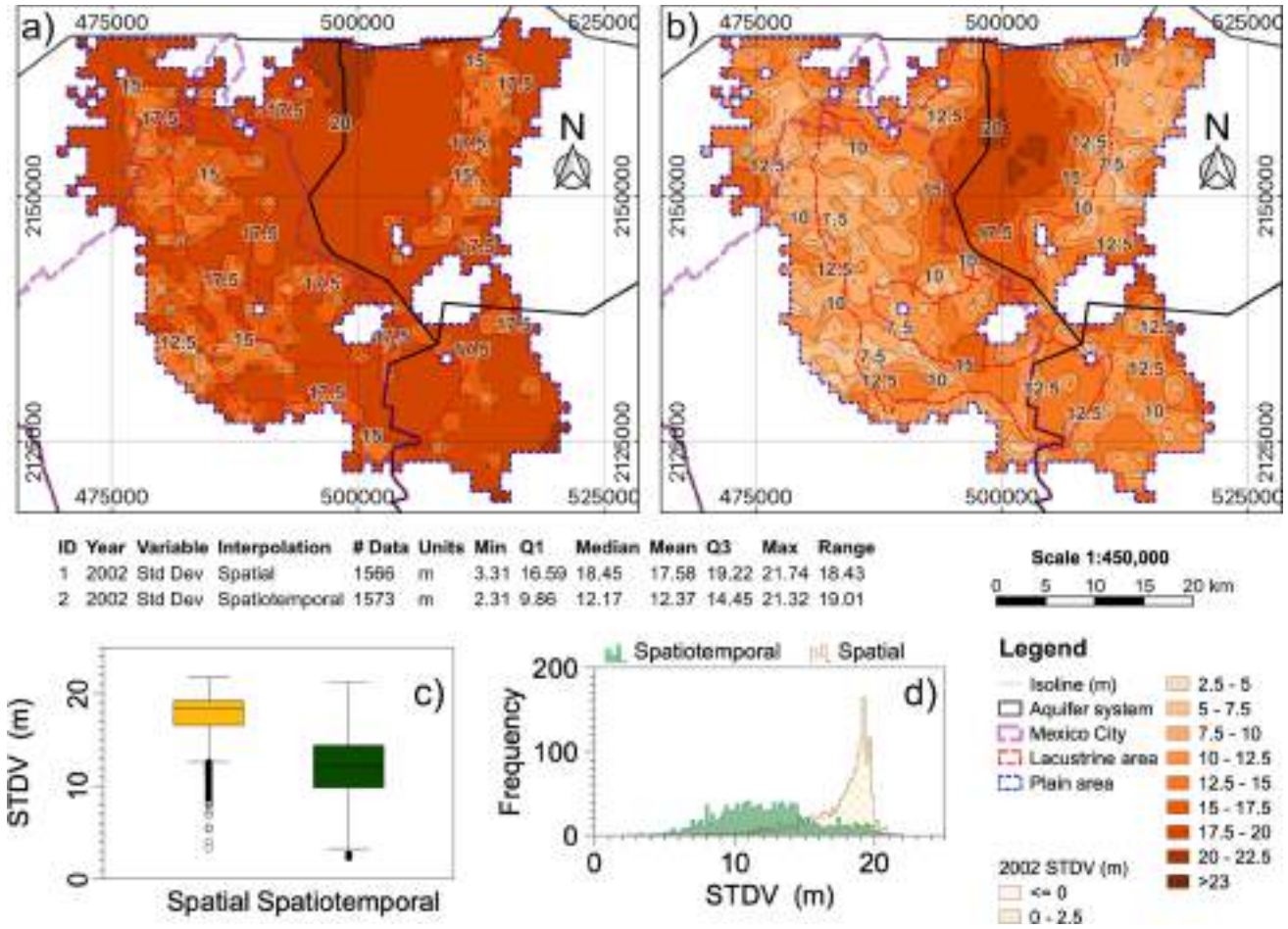

Fig. 10 Comparison of the standard deviation of GE for the year 2002: **a** spatial and **b** ST kriging contour maps, **c** box plots, and **d** histograms

period of analysis, the drawdowns of the groundwater level in the aquifer system is about 1 m/year. In both cases, there are consistent drawdowns between the latitudes 2,130,000 and 2,150,000, almost on a diagonal line that crosses from west to east in the ST kriging map, but only crossing the Texcoco aquifer and a portion of the MMC aquifer in the spatial kriging map. Note that the spatial kriging map has more extended areas with drawdowns larger than 10 m, which is heavily influenced by the available spatial data in years 2002 and 2007.

Checking GE recovery (negative values), 17.3% of the analyzed area is obtained for the ST kriging estimates and 32.5% for the spatial kriging. The last percentage for the spatial kriging provides an implausible pattern for a heavily pumped aquifer. Considering these percentages, the ST kriging recovery and drawdown results for the five years are reasonably smaller than those for the spatial case.

Zones with recoveries of 25 to 40 m (negative values) are observed in the northwestern area for the spatial kriging; on the other hand, they are estimated as drawdowns in the ST case. It is worth noting that both cases correspond to areas with large SDs of the estimation error (Fig. 13a), although smaller for the ST kriging (Fig. 13b).

Figure 13 compares the contour maps for spatial (a) and ST (b) estimation error SD for GE differences and the distribution of their values through their box plots (c) and histograms (d). The SD values are significantly smaller for the ST kriging (as shown in Fig. 13c), which has 75% of the values smaller than 6 m; in contrast, for the spatial case, 75% of the SD values are larger than 17.2 m, and only a few values are less than 6 m. The contour maps (Fig. 13a, b) are similar to the maps of the estimated error SDs of the GEs for 2002 (Fig. 10) and 2007 (Fig. 11). However, the spatial estimated error SD values are of course larger than the ones in 2002 and 2007, since $\mathrm{Var}[E_1(\mathbf{s},2002)-E_2(\mathbf{s},2007)]=\mathrm{Var}[E_1(\mathbf{s},2002)]+\mathrm{Var}[E_2(\mathbf{s},2007)]$, where $E_1(\mathbf{s},t_1)=\widehat{Z}(\mathbf{s},t_1)-Z(\mathbf{s},t_1)$ and $E_2(\mathbf{s},t_2)=\widehat{Z}(\mathbf{s},t_2)-Z(\mathbf{s},t_2)$ are the GE estimation error SD for the position $\mathbf{s}$ and time t_1 and t_2. On the other hand, for the ST case, the estimated error variance of the GE changes is $\mathrm{Var}[E_1(\mathbf{s},2002)-E_2(\mathbf{s},2007)]=\mathrm{Var}[E_1(\mathbf{s},2002)]+\mathrm{Var}[E_2(\mathbf{s},2007)]-2C_{st}[E_1(\mathbf{s},2002),E_2(\mathbf{s},2007)]$; the estimated error SD of the GE changes is reduced more in the ST case

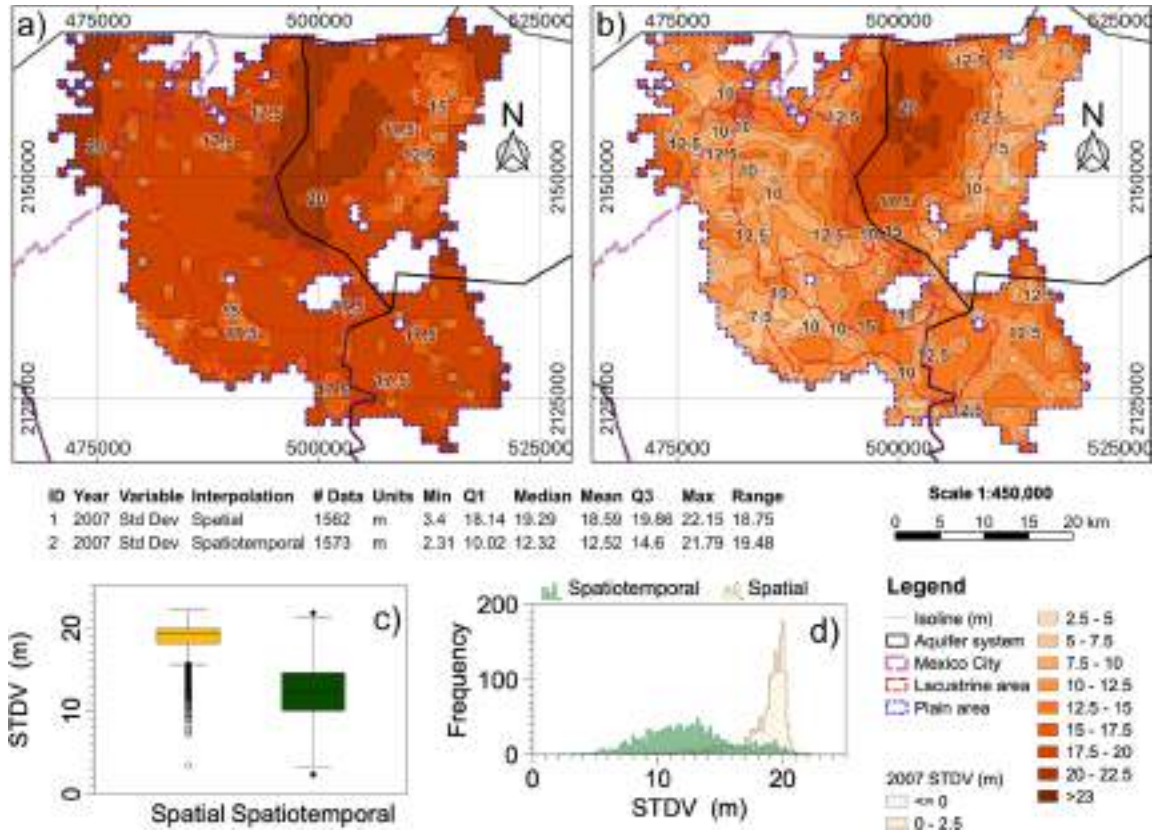

Fig. 11 Comparison of the standard deviation of GE for the year 2007: **a** spatial and **b** ST kriging contour maps, **c** box plots, and **d** histograms

since the covariance between the GE estimate errors at the two years is considered (Fig. 13b).

Uncertainty in the GE change estimates is also checked by computing, for each grid cell, the absolute value of the coefficient of variation (ACV, i.e. the ratios between the SD and the absolute value of the GE difference estimate). 75% of the ACV values are less than 3.5 for the spatial kriging and less than 1.5 for the ST kriging. Therefore, the latter considerably reduces the error estimate uncertainty of the groundwater level change. A complete report of the ACV values is presented in the electronic supplementary material (ESM) and the maps that show details on the spatial distribution differences between the two approaches for the CV and ACV of the GE changes.

Discussion

In previous works, temporal changes in groundwater levels, for a given period, were calculated by using two procedures based on spatial kriging. In the first approach, for each well, the groundwater level in the period's final year is subtracted from the corresponding level in the period's initial year, and afterward, kriging interpolation is done (for example, Ta'Any et al. 2009 and Ahmadi and Sedghamiz 2007). This procedure is possible when the data are available for the initial and final years of the evaluated period at the same wells or if the missing data are filled in. In the second approach, temporal changes are calculated by subtracting the groundwater levels after interpolating each year's data over a spatial grid (for example, Sun et al. 2009). However, when data are unavailable in the same set of wells for the initial and final years of the evaluated period, this approach, although possible, may produce misleading results.

This work proposes an alternative for the second approach, in which the GE interpolation is obtained with ST kriging and then takes advantage of the available observations not only over space, but also in time. Ruybal et al. (2019a) used a similar approach to calculate temporal changes in piezometric levels. However, their emphasis was on analyzing the piezometric levels, and the temporal changes were only presented in maps. On the other hand, Ruybal et al. (2019b) focused on evaluating groundwater storage changes in the Denver Basin Aquifer System (USA), applying the ST approach of their previous work, emphasizing the hydrological implications and highlighting uncertainty in the volumetric predictions on the basis

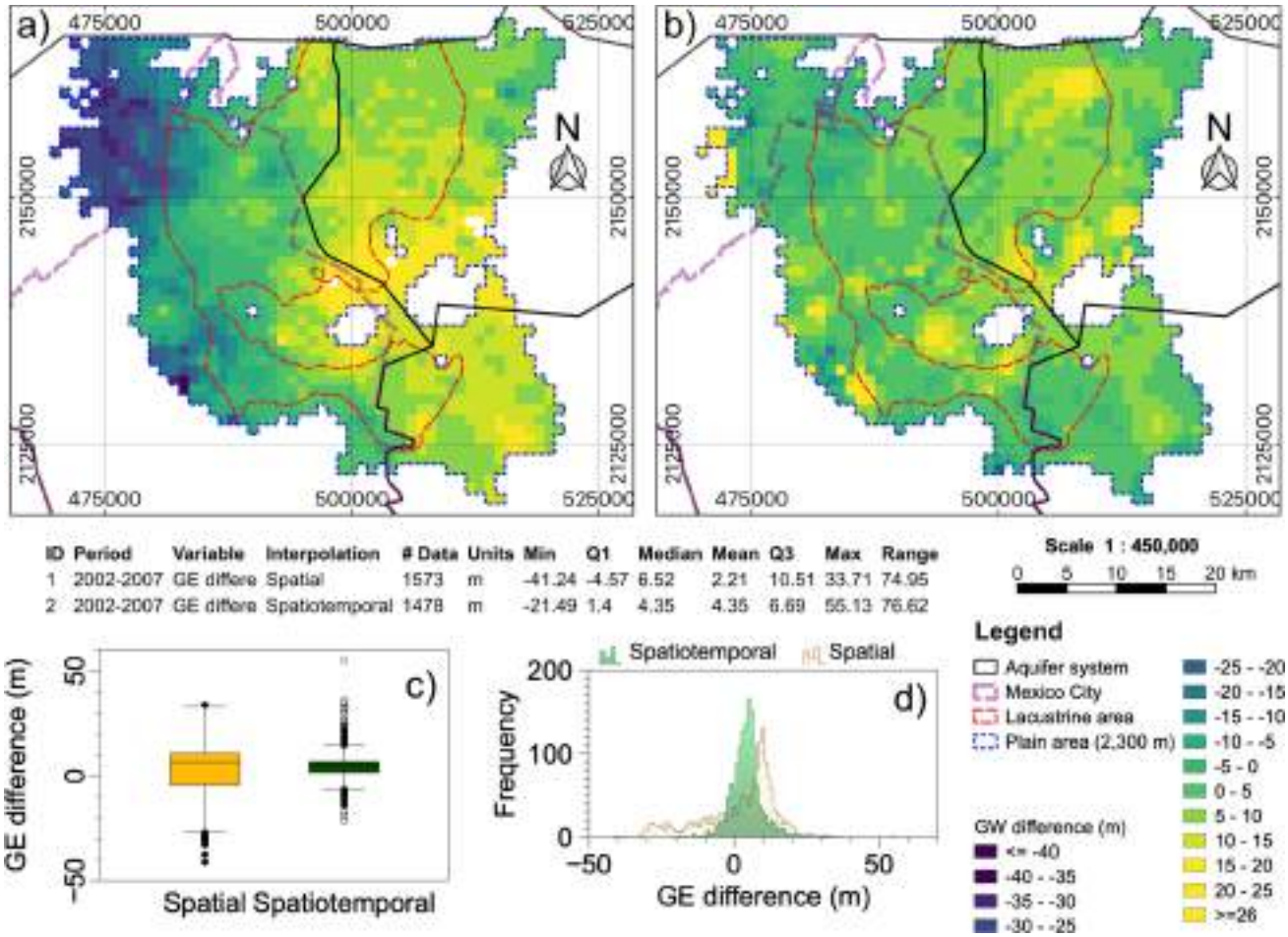

Fig. 12 Comparison of groundwater level temporal changes: **a** spatial and **b** ST kriging contour maps, **c** box plots, and **d** histograms

of the storage coefficient uncertainty. None of these works thoroughly compared the spatial and ST kriging results and the estimated errors of the groundwater level temporal changes, as evaluated in this work. Furthermore, in contrast with Ruybal et al. (2019a), in this work, the non-separability index (Cappello et al. 2018) is used to choose the appropriate class of the ST variogram model. Also, the SD of the estimate errors of the GE temporal change has been computed and presented for the first time using ST kriging. The results have highlighted the improvements in terms of more realistic estimates and reduced estimation error SD, obtained when data at other times are involved in the interpolation process.

Ruybal et al. (2019a) proposed a list of pending issues in the ST geostatistical applications to Hydrogeology (Table 1). These were: (1) assessment of the applicability of additional space-time variogram models to predict groundwater levels; (2) evaluation of aquifers on a larger scale with an extent of thousands of kilometers; (3) further assessment of ST kriging for confined, semiconfined, and unconfined systems; (4) evaluation of longer time periods; (5) evaluation of more methods to remove global groundwater trends or drift; and (6) advocating for the advantages of ST applications on irregular or sparse groundwater datasets, which is common in groundwater applications.

Referring to the above mentioned issues this study has given a significant contribution to the successful application of the ST approach: (i) on a regional aquifer; (ii) on the semiconfined and unconfined conditions in the SBMAS; (iii) by using a long time series length (21 years); (iv) on the irregularly distributed GE dataset (even with broad areas lacking data between the MMC and Texcoco aquifers), where the ST geostatistical application dramatically reduces the uncertainty in the estimation error SD.

Finally, it is worth recalling that in the presented analysis, the trend has been removed from the data, so that the structural analysis and kriging have been conducted on the residuals. Once the estimated residuals have been obtained, the trend is added in order to determine the

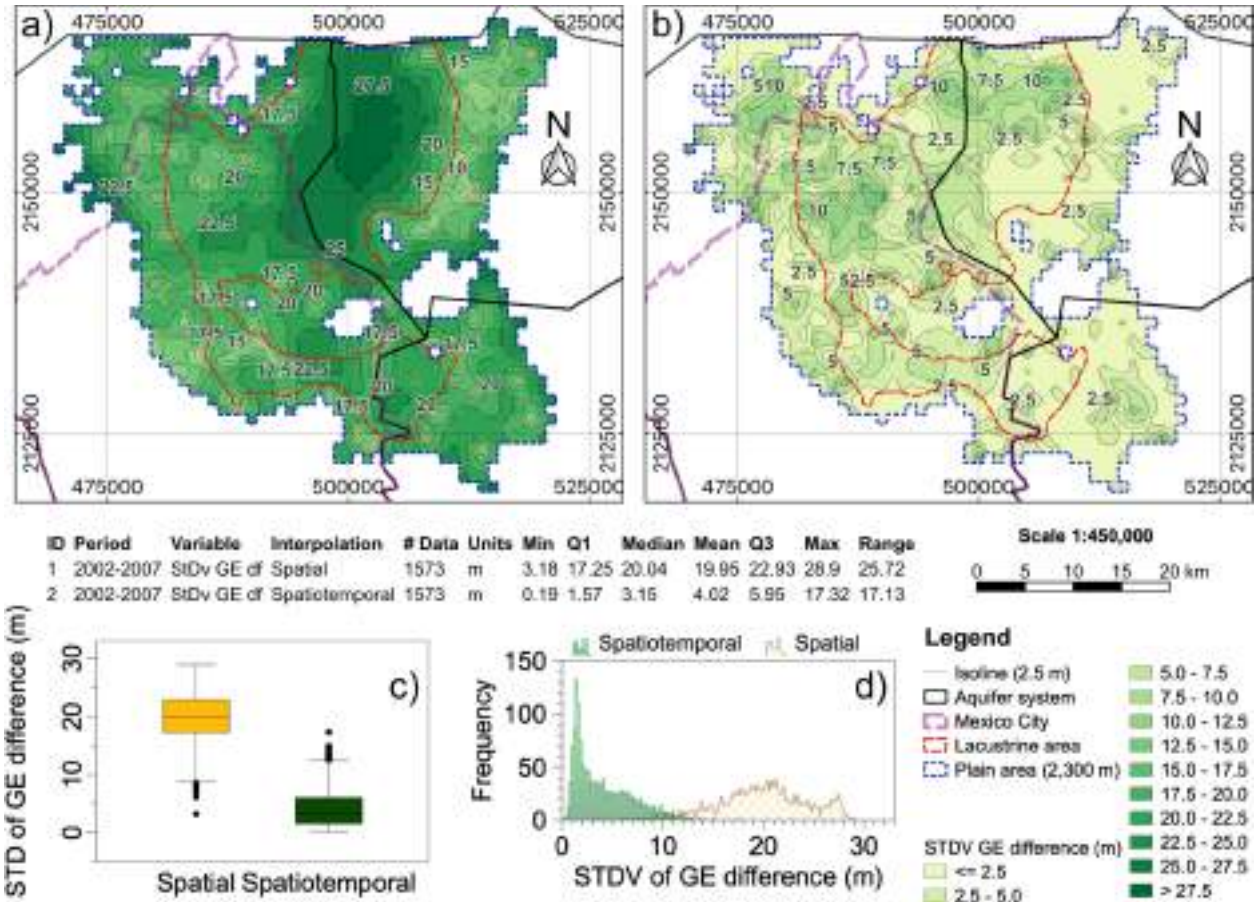

Fig. 13 Comparison of the estimation error SD of the groundwater level difference: **a** spatial and **b** ST kriging contour maps, **c** box plots, and **d** histograms

estimated values for the variable under study. This is a consolidated way to proceed in the presence of a trend, as also shown in the published papers on the same subject referred to in Table 1. However, considering that after subtracting the trend, as done when applying residual kriging, the experimental variogram of the residuals presents a bias (see, for example, Matheron 1971), the adoption of other methods that avoid this problem, like universal kriging or IRF-k kriging, represents a pending issue that could be addressed in future works.

Conclusions

The analysis conducted in this work focused on estimating groundwater level changes in the upper area of the SBMAS. For this aim, the performance of the spatial and ST approaches was evaluated, and estimation error SDs of the GE changes were presented. The improvements of applying the ST kriging for the GE estimates compared to the spatial kriging were quantified on the basis of the cross-validation results and the estimate error SDs, which were useful to better distinguish relevant hydrological behaviors. Especially for the computed differences in the GE, the ST kriging produces more reasonable results than the spatial kriging, since less extreme recoveries and drawdowns, associated to smaller SD of the estimate errors, were highlighted.

A thorough ST hydrogeological analysis of the groundwater level changes for the period 1997 to 2017 in the upper aquifer of the SBMAS and their different sources of uncertainty (including the interpolation error of the groundwater level changes) should be performed in the future. Moreover, the complex geostatistical approach, both in the spatial domain (De Iaco et al. 2003; De Iaco et al. 2013; De Iaco 2017; De Iaco, 2023b) and in the spatio-temporal context (Cappello et al., 2021a, b, 2022; De Iaco, 2022, 2023a), holds significant potential for modeling groundwater velocity, as demonstrated in the work of De Iaco and Posa (2016).

Supplementary Information The online version contains supplementary material available at https://doi.org/10.1007/s10040-023-02681-y.

Funding This research was partially funded by UNAM-PAPIIT IN110620.

Declarations

Conflict of interest The authors declare no conflict of interest.

References

Ahmadi SH, Sedghamiz A (2007) Geostatistical analysis of spatial and temporal variations of groundwater level. Environ Monit Assess 129:277–294. https://doi.org/10.1007/s10661-006-9361-z

Arce JL, Layer PW, Macías JL, Morales-Casique E, García-Palomo A, Jiménez-Domínguez FJ, Benowitz J, Vásquez-Serrano A (2019) Geology and stratigraphy of the Mexico Basin (Mexico City), central Trans-Mexican Volcanic Belt. J Maps 15(2):320–332. https://doi.org/10.1080/17445647.2019.1593251

Ávila-Carrasco JR, Hernández-Hernández MA, Herrera GS, Hernández-García GDJ (2023) Urbanization effects on the groundwater potential recharge of the aquifers in the Southern part of the Basin of Mexico. Hydrol Res. https://doi.org/10.2166/nh.2023.103

Bücker M, Lozano García S, Ortega Guerrero B, Caballero M, Pérez L, Caballero L (2017) Brown E (2017) Geoelectrical and electromagnetic methods applied to paleolimnological studies: two examples from Desiccated Lakes in the Basin of Mexico. Boletín de la Sociedad Geológica Mexicana. 69(2):279–298

Carrillo-Rivera JJ, Cardona A, Huizar-Álvarez R, Graniel E (2008) Response of the interactions between groundwater and other components of the environment in Mexico. Environmental Geology Journal. 55:303–319. https://doi.org/10.1007/s00254-007-1005-2

Cappello C, De Iaco S, Posa D (2018) Testing the type of non-separability and some classes of space-time covariance function models. Stoch Env Res Risk Assess 32:17–35. https://doi.org/10.1007/s00477-017-1472-2

Cappello C, De Iaco S, Posa D (2020) Covatest: An R package for selecting a class of space-time covariance functions. Journal of Statistical Software 94:1–42. https://doi.org/10.18637/jss.v094.i01

Cappello C, De Iaco S, Maggio S, Posa D (2021a) Modeling ocean currents through complex random fields indexed in time. Math Geosci 53:999–1025. https://doi.org/10.1007/s11004-020-09880-3

Cappello C, De Iaco S, Maggio S, Posa D (2021b) Time varying complex covariance functions for oceanographic data. Spat Stat 42:1–17. https://doi.org/10.1016/j.spasta.2020.100426

Cappello C, De Iaco S, Maggio S, Posa D (2022) Modeling spatio-temporal complex covariance functions for vectorial data. Spat Stat 47(100562):1–18. https://doi.org/10.1016/j.spasta.2021.100562

Chilès JP, Delfiner P (2012) Geostatistics: Modeling Spatial Uncertainty. Wiley & Sons Inc, New York

Comisión Nacional del Agua (2018) Actualización de la disponibilidad media anual de agua en el acuífero Zona Metropolitana de la Cd. de México [Update of the average annual availability of water in the Mexico City Metropolitan Area aquifer] (0901), Distrito Federal. Published in the Official Gazette of the Mexican Federation on January 4, 2018

Cressie N (1993) Statistics for Spatial Data. John Wiley & Sons, New York

Christakos G (1984) On the problem of permissible covariance and variogram models. Water Resour Res 20:251–265. https://doi.org/10.1029/WR020i002p00251

Cressie N, Huang HC (1999) Classes of Nonseparable, spatiotemporal Stationary Covariance Functions. J Am Stat Assoc 94(448):1330–1339. https://doi.org/10.1080/01621459.1999.10473885

De Cesare L, Myers DE, Posa D (2001) Estimating and modeling space-time correlation structures. Statist Probab Lett 51:9–14. https://doi.org/10.1016/S0167-7152(00)00131-0

De Iaco S (2017) The cgeostat software for analyzing complex-valued random fields. J Stat Softw 79:1-32. https://doi.org/10.18637/jss.v079.i05

De Iaco S (2022) New spatio-temporal complex covariance functions for vectorial data through positive mixtures. Stoch Environ Res Risk Assess 36:2769–2787. https://doi.org/10.1007/s00477-022-02171-9

De Iaco S (2023a) Spatio-temporal generalized complex covariance models based on convolution. Comput Stat Data Anal 183:107709. https://doi.org/10.1016/j.csda.2023.107709

De Iaco S (2023b) Families of complex-valued covariance models through integration. Environmetrics 34(3):e2779. https://doi.org/10.1002/env.2779

De Iaco S, Myers DE, Posa D (2001) Space-time analysis using a general product-sum model. Statist Probab Lett 52:21–28. https://doi.org/10.1016/S0167-7152(00)00200-5

De Iaco S, Myers DE, Posa D (2002) Nonseparable space-time covariance models: Some parametric families. Math Geol 34(1):23–42. https://doi.org/10.1023/A:1014075310344

De Iaco S, Palma M, Posa D (2003) Covariance functions and models for complex-valued random fields. Stoch Environ Res Risk Assess 17:145–156. https://doi.org/10.1007/s00477-003-0129-5

De Iaco S, Posa D (2013) Positive and negative non-separability for space-time covariance models. J Statist Plan Infer 143:378–391. https://doi.org/10.1016/j.jspi.2012.07.006

De Iaco S, Posa D (2016) Wind velocity prediction through complex kriging: formalism and computational aspects. Environ Ecol Stat 23(1):115–139. https://doi.org/10.1007/s10651-015-0331-x

De Iaco S, Posa D (2018) Strict positive definiteness in geostatistics. Stoch Environ Res Risk Assess 32:577–590. https://doi.org/10.1007/s10651-015-0331-x

De Iaco S, Posa D, Palma M (2013) Complex-valued random fields for vectorial data: estimating and modeling aspects. Math Geosci 45:557–573. https://doi.org/10.1007/s11004-013-9468-z

Durazo J, Farvolden RN (1989) The groundwater regime of the Valley of Mexico from historic evidence and field observations. J Hydrol 112(1–2):171–190. https://doi.org/10.1016/0022-1694(89)90187-X

Gneiting T (2002) Nonseparable, stationary covariance functions for space-time data. J Am Stat Assoc 97(458):590–600

Herrera I, Dumars (1995) "El agua y la Ciudad de México: Abastecimiento y Drenaje, Calidad, Salud Pública, Uso Eficiente, Marco Jurídico e Institucional" ["Water and Mexico City: Supply and Drainage, Quality, Public Health, Efficient Use, Legal and Institutional Framework"]. Consejo Nacional de Investigación (1995) Editado en colaboración con National Academy

of Sciences. México, Comité Nacional de Investigación, US-National Research Council, p 353

Herrera-Zamarrón G, Armienta-Hernández MA, Morales-Arredondo JI, Hernández-Hernández MA, Kohn-Ledesma I, Júnez-Ferreira HE, Arango Galván C, Arce-Saldaña JL, Morales-Casique E, Cortés Silva A (2020) Estudio para la caracterización de la calidad del agua del acuífero de la Ciudad de México. Ciudad de México, México [Study for the characterization of the water quality of the Mexico City aquifer. Mexico City, Mexico]. Sistema de aguas de la Ciudad de México, Instituto de Geofísica de la UNAM. Convenio No. 0266-1O-ED-F-DGAT-UNAM-2-19-1928

Instituto Nacional de Estadística y Geografía (2022) Censo de Población y Vivienda 2022, actualizado el 16 de marzo de 2021 [Population and Housing Census 2022, updated on March 16, 2021]. Consultado en: https://www.inegi.org.mx/programas/ccpv/2020/. Accessed 11 Nov 2022

Journel AG, Huijbregts ChJ (1978) Mining Geostatistics. New York (Academic Press), London, p 600

Kyriakidis PC, Journel AG (1999) Geostatistical space - time models: a review. Math Geol 31:651–684

Ma C (2002) Spatio-temporal covariance functions generated by mixture. Math Geol 34(8):965–975. https://doi.org/10.1023/A:1021368723926

Ma C (2003) Families of spatio-temporal stationary covariance models. J Statist Plan Infer 116:489–501. https://doi.org/10.1016/S0047-259X(02)00014-3

Matheron G (1971) The theory of regionalized variables and its applications. Les cahiers du Centre de Morphologie Mathématique de Fontainebleau, Fasc. 5. Ecole des Mines de Paris

Mendoza-Cázares EY, Herrera-Zamarrón G (2007) Estimación multivariada espacio-tiempo de la carga hidráulica en el valle de Querétaro-Obrajuelo [Multivariate space-time estimation of hydraulic head in the Querétaro-Obrajuelo valley]. Ingeniería Hidráulica en México 22:63–80

Mendoza-Cázares EY, Herrera-Zamarrón G (2010) Estimación espacio-temporal de la carga hidráulica utilizando el concepto de función aleatoria espacio-tiempo [Space-time estimation of hydraulic head using the concept of space-time random function]. Tecnología y Ciencias Del Agua 1:87–111

Mooser F, Molina C (1993) Nuevo modelo hidrogeológico para la cuenca de México [New hydrogeological model for the basin of Mexico]. Boletín del Centro de Investigación Sísmica de la Fundación Javier Barros Sierra, México. 3(1):68–84

Mooser HF, Montiel A, Zúñiga A (1996) Nuevo mapa geológico de las cuencas de México, Toluca y Puebla [New geological map of the basins of Mexico, Toluca and Puebla]. Comisión Federal de Electricidad, México

Ortega Guerrero A, Cherry JA, Aravena R (1997) Origin of pore water and salinity in the lacustrine aquitard overlying the regional aquifer of Mexico City. J Hydrol 197:47–69. https://doi.org/10.1016/S0022-1694(96)03280-5

Posa D (1993) A simple description of spatio-temporal processes. Comput Stat Data Anal 15:425–437. https://doi.org/10.1016/0167-9473(93)90174-R

Rodriguez A, Diggle PJ (2010) A class of convolution-based models for spatio-temporal processes with non-separable covariance structure. Scan J Stat 37(4):553-567

Rodriguez-Iturbe I, Mejía JM (1974) The design of rainfall networks in time and space. Water Resour Res 10:713–728. https://doi.org/10.1029/WR010i004p00713

Rudolph DL, Cherry JA, Farvolden RN (1991) Groundwater flow and solute transport in fractured lacustrine clay near Mexico City. Water Resour Res 27(9):2187–2201. https://doi.org/10.1029/91WR01306

Ruybal CJ, Hogue TS, McCray JE (2019a) Evaluation of groundwater levels in the Arapahoe Aquifer using spatio-temporal regression kriging. Water Resour Res 55:1–18. https://doi.org/10.1029/2018WR023437

Ruybal CJ, Hogue TS, McCray JE (2019b) Assessment of groundwater depletion and implications for management in the Denver Basin Aquifer system. JAWRA Journal of the American Water Resources Association 1752–1688:12755. https://doi.org/10.1111/1752-1688.12755

Sun Y, Kang S, Li F, Zhang L (2009) Comparison of interpolation methods for depth to groundwater and its temporal and spatial variations in the Minqin oasis of northwest China. Environ Model Softw 24(10):1163–1170. https://doi.org/10.1016/j.envsoft.2009.03.009

Ta'Any RA, Tahboub AB, Saffarini GA (2009) Geostatistical analysis of spatiotemporal variability of groundwater level fluctuations in Amman-Zarqa basin, Jordan: A case study. Environ Geol 57(3):525–535. https://doi.org/10.1007/s00254-008-1322-0

Varouchakis EA (2018) Spatiotemporal geostatistical modelling of groundwater level variations at basin scale: a case study at Crete's Mires Basin. Hydrol Res 49(4):1131–1142. https://doi.org/10.2166/nh.2017.146

Varouchakis EA, Theodoridou PG, Karatzas GP (2019) Spatiotemporal geostatistical modeling of groundwater levels under a Bayesian framework using means of physical background. J Hydrol 575:487–498. https://doi.org/10.1016/j.jhydrol.2019.05.055

Varouchakis EA, Guardiola-Albert C, Karatzas GP (2022) Spatiotemporal geostatistical analysis of groundwater level in aquifer systems of complex hydrogeology. Water Resour Res 58(3). https://doi.org/10.1029/2021wr029988

Vázquez-Sánchez E, Jaimes-Palomera R (1989) Geología de la Cuenca de México [Geology of the Basin of Mexico]. Geofisica Internacional 28:133–174